

tegrate seamlessly with it and provide reliable utility under privacy-preserving settings.

Lastly, our framework demonstrates additional advantages in several aspects. It is more communication efficient as multiple optimization rounds can be performed on the server side, and – particularly for large models – transferring synthetic data is less costly than gradients in each round. Beyond the immediate benefits demonstrated in our presentation, we argue that our approach can also lead to more interpretable and inspectable federated learning paradigms and may provide a potential path to reconciling the tension between accountability and privacy in federated learning.

Overall, we summarize our contributions as follows.

- We propose Fed-GLOSS-DP that uses synthetic images to globally approach federated optimization, which has yet to be thoroughly investigated in the past.
- We demonstrate how it finds local approximation and effective approximation regions on clients and performs global federated optimization on the server.
- Fed-GLOSS-DP provides rigorous record-level DP guarantees with reliable utility and outperforms gradient-based counterparts under privacy-preserving settings.
- Experiments verify that our framework better mitigates data heterogeneity. Our method converges significantly faster in non-IID settings and saves up to 85% communication costs.

2. Related Work

Non-IID Data in Federated Learning causes major challenges in FL (Kairouz et al., 2021). Existing efforts mainly fall into the following categories: variance-reduction techniques (Karimireddy et al., 2020; Yu et al., 2019), constraining the dissimilarity between clients’ updates (Li et al., 2020a; 2021), and adjusting the global model to a personalized version at the inference stage (Luo et al., 2021; Li et al., 2020b). In contrast, we present a novel perspective to this challenge by resembling the global loss landscape and performing optimization from a comprehensive view.

Dataset Distillation Our work is largely motivated by recent progress in distilling the necessary knowledge of model training into a small set of synthetic samples (Wang et al., 2018; Zhao et al., 2020; 2021; Zhao and Bilen, 2023; Cazenavette et al., 2022). Our approach is built on top of DSC (Zhao et al., 2021) with several key differences. The proposed Fed-GLOSS-DP (i) focuses on finding local approximation and assembling the global loss landscape to facilitate federated optimization, (ii) is class-agnostic and complements record-level differential privacy while prior work often considers class-wise alignment and could cause privacy risks, and (iii) is designed for multi-round training with several critical design choices. The most similar work

is Chen et al. (2022). They also consider class-agnostic distillation and differential privacy while focusing on one-round distillation rather than multiple-round federated learning.

3. Background

3.1. Federated Learning

In federated learning, we consider training a model \mathbf{w} that maps the input \mathbf{x} to the output prediction y . We assume K clients participate in the training, and each owns a private dataset \mathcal{D}_k with distribution p_k . We use the subscript k to represent the indices of clients, and the superscript m and t to denote the m -th communication round and t -th local step, respectively, unless stated otherwise.

Overall, the learning objective is to find the optimal model \mathbf{w} that minimizes the empirical global loss over the population distribution:

$$\mathcal{L}(\mathbf{w}) = \mathbb{E}_{\mathbf{x}, y \sim p}[\ell(\mathbf{w}, \mathbf{x}, y)] = \frac{1}{N} \sum_{j=1}^N \ell(\mathbf{w}, \mathbf{x}^j, y^j) \quad (1)$$

where ℓ could be arbitrary loss criteria such as cross-entropy and N is the total dataset size. However, in the federated setting, direct access to the global objective is prohibited as all client data is stored locally. Instead, the optimization is conducted on local surrogate objectives $\mathcal{L}_k(\mathbf{w})$:

$$\mathcal{L}(\mathbf{w}) = \sum_{k=1}^K \frac{N_k}{N} \mathcal{L}_k(\mathbf{w}), \quad \mathcal{L}_k(\mathbf{w}) = \sum_{j=1}^{N_k} \frac{1}{N_k} \ell(\mathbf{w}, \mathbf{x}^j, y^j),$$

where (\mathbf{x}^j, y^j) are data samples from the client dataset \mathcal{D}_k .

Existing methods, such as FedAvg (McMahan et al., 2017), simulate stochastic gradient descent on the global objective by performing local gradient updates and periodically aggregating and synchronizing them on the server side. Specifically, at the m -th communication round, the server broadcasts the current global model weights $\mathbf{w}_g^{m,1}$ to each client, who then perform T local iterations with learning rate η .

$$\mathbf{w}_k^{m,1} \leftarrow \mathbf{w}_g^{m,1}, \forall k \in [K] \quad (2)$$

$$\mathbf{w}_k^{m,t+1} = \mathbf{w}_k^{m,t} - \eta \nabla \mathcal{L}_k(\mathbf{w}_k^{m,t}), \forall t \in [T] \quad (3)$$

The local updates $\Delta \mathbf{w}_k^m$ are then sent back to the server and combined to construct the final global update \mathbf{g}^m :

$$\mathbf{g}^m = \sum_{k=1}^K \frac{N_k}{N} \Delta \mathbf{w}_k^m = \sum_{k=1}^K \frac{N_k}{N} (\mathbf{w}_k^{m,T} - \mathbf{w}_k^{m,1}) \quad (4)$$

$$\mathbf{w}_g^{m+1,1} = \mathbf{w}_g^{m,1} - \eta \mathbf{g}^m \quad (5)$$

3.2. Non-IID Challenges

The heterogeneity of client data distribution presents several major challenges to FL, such as a significant decrease in the convergence speed (and even divergence), and a drastic drop in the final performance when compared to the standard IID training setting (Khaled et al., 2019; Li et al., 2020a; Karimireddy et al., 2020; Li et al., 2019). This can be easily seen from the mismatch between the local objectives that is being solved and the global objective that we are indeed aiming for, i.e., $\mathcal{L}_k(\mathbf{w}) \neq \mathbb{E}_{\mathbf{x}, y \sim p}[\ell(\mathbf{w}, \mathbf{x}, y)]$ if $p_k \neq p$ for some k . Running multiple local steps on the local objective (Eq. 3) makes the local update $\Delta \mathbf{w}_k^m$ deviate heavily from the true global gradient $\nabla \mathcal{L}(\mathbf{w})$, inevitably resulting in a biased approximation of the global gradient via Eq. 4 (See Fig. 1 for a demonstration.).

While significant advances have been achieved by existing works in alleviating divergence issues, these methods still exhibit bias towards optimizing the global objective as they rely on the submitted client updates $\Delta \mathbf{w}_k^m$, which only indicate the direction towards the client’s local optimum rather than the global one. In contrast, our method communicates the synthetic samples \mathcal{S}_k , which encode the local optimization landscapes, i.e., gradient directions around possible trajectories $(\mathbf{w}_k^{m,1}, \mathbf{w}_k^{m,2}, \dots, \mathbf{w}_k^{m,T})$, rather than a single direction $\Delta \mathbf{w}_k^m = \mathbf{w}_k^{m,T} - \mathbf{w}_k^{m,1}$ as done in existing works. This fundamental change provides the central server with a global perspective that more faithfully approximates the ground-truth global optimization (See Fig. 1 top row) than existing approaches. Moreover, unlike previous work that need to sacrifice communication efficiency for (Yu et al., 2019) transmitting extra information (e.g., momentum) about local optimization, our approach even improve the communication efficiency by condensing the information into a small set of representative samples, with the total dimension $\dim(\mathcal{S}_k) \ll \dim(\Delta \mathbf{w}_k^m)$.

3.3. Differential Privacy

Differential Privacy (DP) provides strong guarantees of privacy protection while allowing for quantitative measurement of utility. We review several definitions used in this work in this section.

Definition 3.1 (Differential Privacy (Dwork et al., 2014)). A randomized mechanism \mathcal{M} with range \mathcal{R} satisfies (ϵ, δ) -differential privacy, if for any two adjacent datasets E and E' , i.e., $E' = E \cup \{x\}$ for some x in the data domain (or vice versa), and for any subset of outputs $O \subseteq \mathcal{R}$, it holds that

$$\Pr[\mathcal{M}(E) \in O] \leq e^\epsilon \Pr[\mathcal{M}(E') \in O] + \delta \quad (6)$$

In Federated Learning, the notion of *adjacent (neighboring) datasets* used in DP generally refers either to pairs of

datasets differing by one user (*user-level* DP) or by one data point of one user (*record-level* DP). Our work focuses on the latter. Although there are approaches that provide record-level DP for training federated models (Truex et al., 2019; Peterson et al., 2019; Kerkouche et al., 2021), they still suffer from non-IID data. Our method is more robust in training stability and utility.

Intuitively, DP guarantees that an adversary, provided with the output of \mathcal{M} , can draw almost the same conclusions (up to ϵ with probability larger than $1 - \delta$) about any record no matter if it is included in the input of \mathcal{M} or not (Dwork et al., 2014). This means, for any record owner, a privacy breach is unlikely to be due to its participation in the dataset.

We use the Gaussian mechanism to upper bound privacy leakage when transmitting information from clients to the server.

Definition 3.2. (Gaussian Mechanism (Dwork et al., 2014)) Let $f : \mathbb{R}^n \rightarrow \mathbb{R}^d$ be an arbitrary function that maps n -dimensional input to d logits with sensitivity being

$$\Delta_2 f = \max_{E, E'} \|f(E) - f(E')\|_2 \quad (7)$$

over all adjacent datasets E and $E' \in \mathcal{E}$. The Gaussian Mechanism \mathcal{M}_σ , parameterized by σ , adds noise into the output, i.e.,

$$\mathcal{M}_\sigma(x) = f(x) + \mathcal{N}(0, \sigma^2 I). \quad (8)$$

\mathcal{M}_σ is (ϵ, δ) -DP for $\sigma \geq \sqrt{2 \ln(1.25/\delta)} \Delta_2 f / \epsilon$.

As in Abadi et al. (2016); Mironov et al. (2019), we consider in this work, the Sampled Gaussian Mechanism (SGM)—a composition of subsampling and the additive Gaussian noise (defined in A.3)—for privacy amplification. Moreover, we first compute the SGM’s Renyi Differential Privacy as in Mironov et al. (2019) and then we use conversion Theorem A.6 from Balle et al. (2020) for switching back to Differential Privacy (See Section A for more details).

Lastly, using the following theorem, our framework can enhance approximation quality without introducing additional privacy budgets.

Theorem 3.3. (Post-processing (Dwork et al., 2014)) If \mathcal{M} satisfies (ϵ, δ) -DP, $G \circ \mathcal{M}$ will satisfy (ϵ, δ) -DP for any data-independent function G .

4. Fed-GLOSS-DP: Federated, Global Learning using Synthetic Sets

4.1. Overview

Unlike existing approaches that typically communicate the local update directions to approximate the optimization of the global objective (Eq. 4), we propose to directly simulate

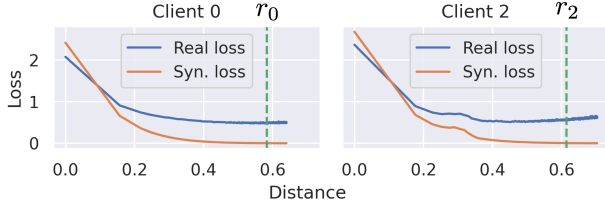


Figure 2. r_k selection. The losses on private real and synthetic data decrease initially but start deviating later. We return the turning points as r_k , i.e., the point corresponds to the smallest real loss, indicating the most effective approximation region.

the global optimization by transmitting a small set of synthetic samples that reflect the local loss landscapes (Fig. 1). Such synthetic data can then be leveraged by the central server as if it were the real data, allowing the training process to mimic the ground-truth global optimization as if we had access to the complete client data distribution.

Let p_k and the p_{S_k} be the distribution of the real client dataset \mathcal{D}_k and the corresponding synthetic dataset \mathcal{S}_k respectively. Our objective can be formalized as:

$$\mathbb{E}_{(\mathbf{x}, y) \sim p_k} [\ell(\mathbf{w}, \mathbf{x}, y)] \simeq \mathbb{E}_{(\hat{\mathbf{x}}, \hat{y}) \sim p_{S_k}} [\ell(\mathbf{w}, \hat{\mathbf{x}}, \hat{y})] \quad (9)$$

The server can then recover the true global objective by:

$$\mathcal{L}(\mathbf{w}) = \sum_{k=1}^K \frac{N_k}{N} \mathcal{L}_k(\mathbf{w}) \simeq \sum_{k=1}^K \frac{N_k}{N} \hat{\mathcal{L}}_k(\mathbf{w}) \quad (10)$$

with $\mathcal{L}_k(\mathbf{w})$ being the left-hand side of Eq. 9 and $\hat{\mathcal{L}}_k(\mathbf{w}) = \frac{1}{|S_k|} \sum_{j=1}^{|S_k|} \ell(\mathbf{w}, \hat{\mathbf{x}}_j, \hat{y}_j)$ the right-hand side. Performing global updates is then equivalent to conducting vanilla gradient descent on the recovered global objective, i.e., by training on the synthetic set of samples.

We demonstrate our framework in Fig. 1. In every communication round, synthetic samples are optimized to approximate the client’s local loss landscapes and then transmitted to the server. The server then performs global updates on the synthetic samples to simulate global optimization.

In the following, we explain how to construct the synthetic datasets on each client that encode the local loss landscapes (Sec 4.2) and how to optimize the global model over a reconstructed loss landscape on the server (Sec 4.3). Lastly, we show in Sec 4.4 that our method is seamlessly compatible with *record-level* differential privacy. The overall algorithm is depicted in Algorithm 1.

4.2. Local Approximation

The goal of this step is to construct a synthetic set of samples \mathcal{S}_k that accurately captures necessary local information for subsequent global updates. A natural approach would be to

Algorithm 1 Fed-GLOSS

function ServerExecute:

Initialize global weight $\mathbf{w}_g^{1,1}$, radius r

/ Local approximation */*

for $m = 1, \dots, M$ **do**

for $k = 1, \dots, K$ **do**

$\mathcal{S}_k, r_k \leftarrow \text{ClientsExecute}(k, r, \mathbf{w}_g^{m,1})$

end for

/ Global optimization */*

$r_g \leftarrow \min\{r_k\}_{k=1}^K$

$t \leftarrow 1$

while $\|\mathbf{w}_g^{m,1} - \mathbf{w}_g^{m,t}\| < r_g$ **do**

$\mathbf{w}_g^{m,t+1} = \mathbf{w}_g^{m,t} - \sum_{k=1}^K \eta \frac{N_k}{N} \nabla_{\mathbf{w}} \mathcal{L}(\mathbf{w}_g^{m,t}, \mathcal{S}_k)$

$t \leftarrow t + 1$

end while

$\mathbf{w}_g^{m+1,1} \leftarrow \mathbf{w}_g^{m,t}$

end for

Return: global model weight $\mathbf{w}_g^{M+1,1}$

function ClientExecute($k, r, \mathbf{w}_g^{m,1}$):

Initialize \mathcal{S}_k : $\{\hat{\mathbf{x}}_k^m\}$ from Gaussian noise or $\{\hat{\mathbf{x}}_k^{m-1}\}$, $\{\hat{y}_k\}$ to be a balanced set

for $i = 1, \dots, R_i$ **do**

/ Resample training trajectories */*

Reset $t \leftarrow 1$ and model $\mathbf{w}_k^{m,1} \leftarrow \mathbf{w}_g^{m,1}$

while $\|\mathbf{w}_k^{m,t} - \mathbf{w}_k^{m,1}\| < r$ **do**

/ Compute the real gradient */*

Sample real data batches $\{(\mathbf{x}_k, y_k)\}$ from \mathcal{D}_k

Compute $g^{\mathcal{D}} = \nabla \mathcal{L}(\mathbf{w}_k^{m,t}, \{(\mathbf{x}_k, y_k)\})$

for $j = 1, \dots, R_b$ **do**

/ Update synthetic set \mathcal{S}_k */*

$\mathcal{S}_k = \mathcal{S}_k - \tau \nabla_{\mathcal{S}_k} \mathcal{L}_{dis}(g^{\mathcal{D}}, \nabla \mathcal{L}(\mathbf{w}_k^{m,t}, \mathcal{S}_k))$

end for

for $l = 1, \dots, R_l$ **do**

/ Update local model parameter \mathbf{w}_k */*

$\mathbf{w}_k^{m,t+1} = \mathbf{w}_k^{m,t} - \eta \nabla \mathcal{L}(\mathbf{w}_k^{m,t}, \mathcal{S}_k)$

$t \leftarrow t + 1$

end for

end while

end for

Measure r_k on \mathcal{D}_k (See Fig. 2)

Return: Synthetic set \mathcal{S}_k , calibrated radius r_k

enforce similarity between the gradients obtained from the real client data and those obtained from the synthetic set:

$$\nabla_{\mathbf{w}} \mathbb{E}_{(\mathbf{x}, y) \sim p_k} [\ell(\mathbf{w}, \mathbf{x}, y)] \simeq \nabla_{\mathbf{w}} \mathbb{E}_{(\hat{\mathbf{x}}, \hat{y}) \sim p_{S_k}} [\ell(\mathbf{w}, \hat{\mathbf{x}}, \hat{y})]$$

We achieve this by minimizing the distance between the gradients:

$$\arg \min_{\mathcal{S}_k} \mathcal{L}_{dis}(\nabla \mathcal{L}(\mathbf{w}, \mathcal{D}_k), \nabla \mathcal{L}(\mathbf{w}, \mathcal{S}_k)) \quad (11)$$

where we denote $\nabla\mathcal{L}(\mathbf{w}, \mathcal{D}_k)$ the stochastic gradient of network parameters on the client dataset \mathcal{D}_k , and $\nabla\mathcal{L}(\mathbf{w}, \mathcal{S}_k)$ the gradient on the synthetic set for brevity. Following existing literature (Zhao et al., 2020; 2021), we adopt a layer-wised cosine distance for \mathcal{L}_{dis} (See appendix for more details).

While solving Eq. 11 for every possible \mathbf{w} would lead to perfect recovery of the ground-truth global optimization in principle, in practice, however, it is infeasible due to the large space of (infinitely many) possible values of \mathbf{w} . Additionally, as $|\mathcal{S}_K|$ is set to be much smaller than N_k (for the sake of communication efficiency), an exact solution may not exist, resulting in approximation error for some \mathbf{w} . To address this, we explicitly constrain the problem space to be the most achievable region for further global updates. Specifically, we consider \mathbf{w}_k that is sufficiently close to the initial point of the local update (Eq. 13) and is located on the update trajectories (Eq. 14). Formally,

$$\arg \min_{\mathbf{S}_k} \sum_{t=1}^T \mathcal{L}_{\text{dis}} \left(\nabla\mathcal{L}(\mathbf{w}_k^{m,t}, \mathcal{D}_k), \nabla\mathcal{L}(\mathbf{w}_k^{m,t}, \mathcal{S}_k) \right) \quad (12)$$

$$\text{s.t.} \quad \|\mathbf{w}_k^{m,t} - \mathbf{w}_k^{m,1}\| < r \quad (13)$$

$$\mathbf{w}_k^{m,t+1} = \mathbf{w}_k^{m,t} - \eta \nabla\mathcal{L}(\mathbf{w}_k^{m,t}, \mathcal{S}_k) \quad (14)$$

In the m -th communication round, the clients first synchronize the local model $\mathbf{w}_k^{m,1}$ with the global model $\mathbf{w}_g^{m,1}$ and initialize the synthetic features $\{\hat{\mathbf{x}}_k^m\}$ either from Gaussian noise or to be the ones obtained from the previous round $\{\hat{\mathbf{x}}_k^{m-1}\}$. Synthetic labels $\{\hat{y}_k\}$ are initialized to be a fixed, balanced set and are not optimized during the training process. The number of synthetic samples $|\mathcal{S}_k|$ is kept equal for all clients in our experiments, though it can be adjusted for each client depending on factors such as local dataset size and bandwidth in practice.

To simulate the local training trajectories, the clients alternate between updating synthetic features (by performing gradient descent of Eq. 12 w.r.t. $\hat{\mathbf{x}}_k$) and updating the local model using Eq. 14. This continues until the current local model weight $\mathbf{w}_k^{m,t}$ is no longer closed to the initial point, as determined by the Euclidean distance on the flattened weight vectors being greater than a pre-defined radius r . Additionally, an appropriate radius r should reflect the overall training progress and the client’s training status, e.g., it should decrease when the global training is close to convergence and should be small for some clients with data that is hard to fit. Thus, we suggest calibrating the radius based on the training progress at each client, as illustrated in Fig. 2. For the DP training setting, we make the choice of r_k data-independent (See Sec. 4.4).

4.3. Global Optimization

Once the server received the synthetic set \mathcal{S}_k and the calibrated radius r_k , global updates can be performed by conducting gradient descent directly on the synthetic set of samples. The global objective can be recovered by $\hat{\mathcal{L}}_k(\mathbf{w})$ according to Eq. 10 (i.e., training on the synthetic samples), while the scaling factor $\frac{N_k}{N}$ can be treated as the scaling factor of the learning rate when computing the gradients on samples from each synthetic set \mathcal{S}_k , namely:

$$\mathbf{w}_g^{m,t+1} = \mathbf{w}_g^{m,t} - \sum_{k=1}^K \eta \cdot \frac{N_k}{N} \nabla_{\mathbf{w}} \mathcal{L}(\mathbf{w}_g^{m,t}, \mathcal{S}_k) \quad (15)$$

$$\text{s.t.} \quad \|\mathbf{w}_g^{m,t} - \mathbf{w}_g^{m,1}\| \leq \min \{r_k\}_{k=1}^K \quad (16)$$

The constraint in Eq. 16 enforces that the global update respect the vicinity suggested by the clients, meaning updates are only made within regions where the approximation is sufficiently accurate.

4.4. Record-level DP

Record-level DP is vital in FL applications, especially for the cross-silo setting. For example, in a collaboration between hospitals, participants attempt to take advantage of others’ data to improve their models while being prohibited from leaking patients’ privacy. The notion of record-level DP can rigorously limit privacy leakage about individuals in such cases. In particular, we consider the following threat model in this work.

Privacy and Adversarial Models. In a federated system, there may be one or multiple colluding adversaries who can access update vectors from any party during each round of training protocol. These adversaries may have infinite computation power while staying passive or so-called honest-but-curious, meaning they faithfully follow the learning protocol and never modifies any update vectors (Truex et al., 2019; Peterson et al., 2019; Kerkouche et al., 2021). Meanwhile, these adversaries could be any participating party, such as a malicious client or server, attempting to infer information from other parties.

Operation. We integrate record-level DP into Fed-GLOSS to provide theoretical privacy guarantees, which yields Fed-GLOSS-DP. Given a desired privacy budget (ϵ, ϵ) , we sanitize the gradients obtained from real data with the Gaussian mechanism, denoted by $\nabla\tilde{\mathcal{L}}(\mathbf{w}_k^{m,t}, \mathcal{D}_k)$. The DP-guaranteed local approximation can be realized by replacing the learning target of Eq. 12 with the sanitized gradients

while leaving other constraints the same. Formally, we have

$$\begin{aligned}
 \arg \min_{\mathcal{S}_k} & \sum_{t=1}^T \mathcal{L}_{\text{dis}} \left(\nabla \tilde{\mathcal{L}}(\mathbf{w}_k^{m,t}, \mathcal{D}_k), \nabla \mathcal{L}(\mathbf{w}_k^{m,t}, \mathcal{S}_k) \right) \\
 \text{s.t.} & \quad \|\mathbf{w}_k^{m,t} - \mathbf{w}_k^{m,1}\| < r \\
 & \quad \mathbf{w}_k^{m,t+1} = \mathbf{w}_k^{m,t} - \eta \nabla \mathcal{L}(\mathbf{w}_k^{m,t}, \mathcal{S}_k).
 \end{aligned}
 \tag{17}$$

We detail how to generate sanitized gradients in Algorithm 2. Our work differentiates itself from Chen et al. (2022) in two points. First, in contrast to single-shot distillation, our method is specifically designed for multiple-round training by approximating the loss surface in an r neighborhood around the *current* parameter $\mathbf{w}_k^{m,t}$. Second, we design an extra iteration R_b over the updates of the synthetic set \mathcal{S}_k and exploit Theorem 3.3 to enhance approximation quality without introducing additional privacy costs.

We additionally provide a privacy analysis of Fed-GLOSS-DP in Sec A due to the space limit.

5. Experiments

5.1. Setup

Datasets, models, and settings. We consider federated learning under non-IID settings. We choose a classification task with ConvNets (LeCun et al., 2010) and three benchmark datasets: MNIST (LeCun et al., 1998), FashionMNIST (Xiao et al., 2017), and CIFAR-10 (Krizhevsky et al., 2009). We construct a non-IID setting in which five clients own disjoint class sets. In other words, each client has two unique classes, which is typically considered a challenging setting (Hsu et al., 2019). In our experiments, we adopt a cross-silo setting (Kairouz et al., 2021), i.e., all clients participate in training in every communication round. The setting is practical, especially for applications such as collaboration between hospitals, where every client owns relatively more but statistically different data.

Implementation. For the baselines, we use a learning rate of 0.1 with cosine decay and run it for 200 epochs. Our method uses a rate of 0.1 to update synthetic images and 0.01 with a decay of every 10 epochs by a factor of 0.5 to update models. We set R_i , R_b , and R_l to be $\{100, 1, 5\}$ in non-private settings and $\{4, 5, 2\}$ in private settings, respectively. We follow Zhao et al. (2021) and assign ten synthetic images to every class unless stated otherwise.

5.2. Data Heterogeneity

We compare Fed-GLOSS to FedAvg (McMahan et al., 2017), the most common gradient-based optimization framework, on MNIST, FashionMNIST, and CIFAR-10. Fig. 3 shows that our method learns much faster than FedAvg and

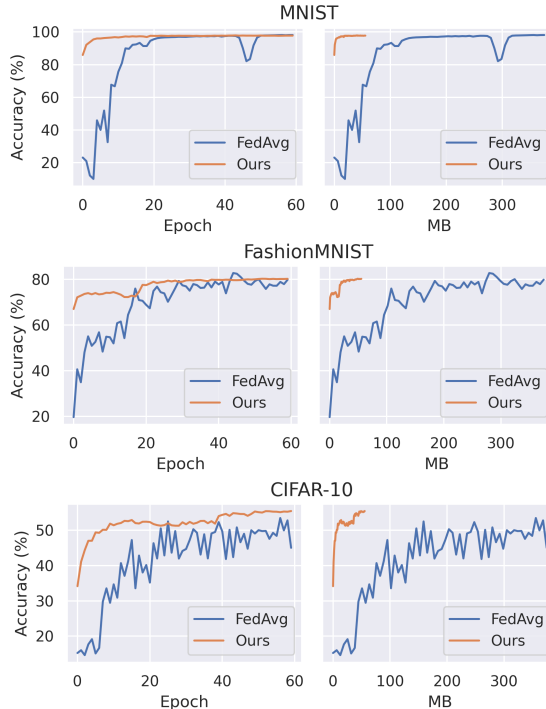


Figure 3. Accuracy over communication rounds and costs of Fed-GLOSS compared to FedAvg with extremely non-IID data.



Figure 4. Hybrid optimization on CIFAR-10.

is not affected by data heterogeneity. In addition, our framework optimizes models from a comprehensive global view and improves more stably while FedAvg tends to fluctuate, which could be unfavorable in practice. Another focus of FL is its communication costs. Our method saves around 85% communication costs to achieve comparable performance at the earlier stage of training. These results conclude that our framework benefits when having non-IID data, limited bandwidth, or even limited training rounds.

5.3. Hybrid Optimization

We demonstrate a hybrid optimization method by combining our method with FedAvg. This approach improves the performance and stability of gradient-based methods. In Fig. 4, we take the checkpoints of our framework at epochs 5, 15, 30, and 60 as initial models and continue with FedAvg. We observe that models pretrained with our method are more stable than random initialization, and models ini-

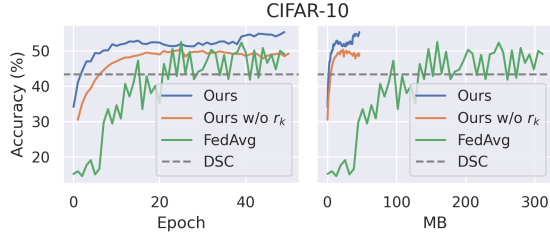


Figure 5. Ablation study on radius selection.

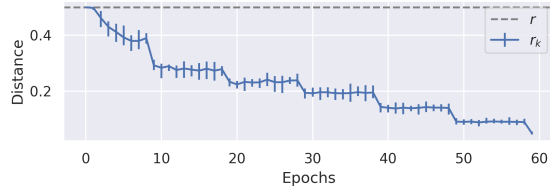


Figure 6. Radius r_k changes vs. the pre-defined radius r over training rounds. The bars indicate the minimum and maximum of the radius, and the curve is plotted based on the mean values. The radius r_k tends to be stable unless the learning changes.

tialized with different checkpoints converge to a similar point around 65%. It suggests that having a global view at an earlier stage helps the overall optimization, even if our method runs only for a few rounds, and is particularly suitable for limited training resources. However, we also notice a performance gap between pure FedAvg and our hybrid method. We hypothesize it might come from the core algorithm of dataset distillation, which is still an ongoing research area.

5.4. Ablation Study

Radius Selection. As discussed in Sec. 4, the server benefits from the radius $\{r_k\}_{k=1}^K$ suggested by the clients. We verify it in Fig. 5. We observe that Fed-GLOSS with the suggested radius outperforms the one without the radius, denoted by *Ours w/o r_k* . However, *Ours w/o r_k* still outperforms FedAvg, suggesting that approaching optimization from a global view alleviates data heterogeneity. We further visualize the radius change over training rounds in Fig. 6. The best radii are roughly stable and change only when we decay the learning rate. Although we provide a data-driven

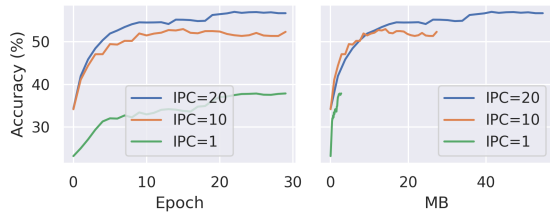
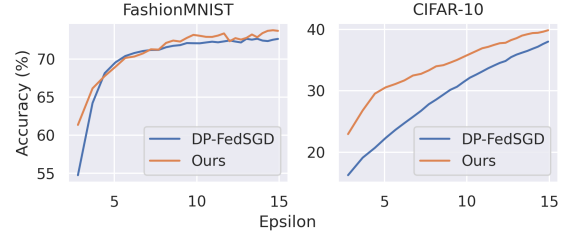


Figure 7. Performance on CIFAR-10 with various numbers of images per class (IPC).


 Figure 8. Privacy vs. utility trade-off with $\delta = 10^{-5}$

approach, the Fig implies that the radii are not highly correlated with data and can be set via heuristics, which is useful for privacy concerns.

Image per Class (IPC). Unlike prior work (Wang et al., 2022; He et al., 2021), our method naturally introduces a trade-off between communication costs and performance, which is missing in the classical gradient-based methods. In addition to the common setting of Zhao et al. (2021), we show that Fed-GLOSS works with different IPC settings. Fig. 7 presents that our method can achieve around 4% higher performance and converge faster by assigning ten more images to every class. It aligns with our motivation that more synthetic images carry more essential information for the server to resemble the global loss landscape.

5.5. Privacy Protection

We evaluate the trade-off between utility and privacy budgets ϵ on FashionMNIST and CIFAR-10 and compare Fed-GLOSS-DP to DP-FedSGD (Truex et al., 2019; Peterson et al., 2019). For a fair comparison, we adapt our method to consume the same privacy cost in every communication round as DP-FedSGD. Specifically, the DP-FedSGD runs five local epochs before communicating with the server and each of which has 40 batches of size 256. Therefore, we set R_i, R_b to $\{4, 5\}$, limit the number of the while loops to five, and samples ten batches in each loop such that it has the same cost as DP-FedSGD. Note that this upper-bounds the privacy leakage of our method since it could terminate earlier if it exceeds the predefined radius r . We consider a noise scale $\sigma = 1$ for both approaches and record the utility over training. More rounds lead to higher utility while consuming more privacy costs. From Fig. 8, we find our framework yields better performance, especially when considering a tighter constraint, i.e., a small ϵ , and the colorful dataset CIFAR-10. In addition to utility, it is worth noting that our method consumes 85% fewer communication costs at the same privacy cost.

5.6. Qualitative Results

We visualize the synthetic images and analyze the distribution of pixel values in this section. Fig. 9 presents the distribution of pixels values of all synthetic images for the

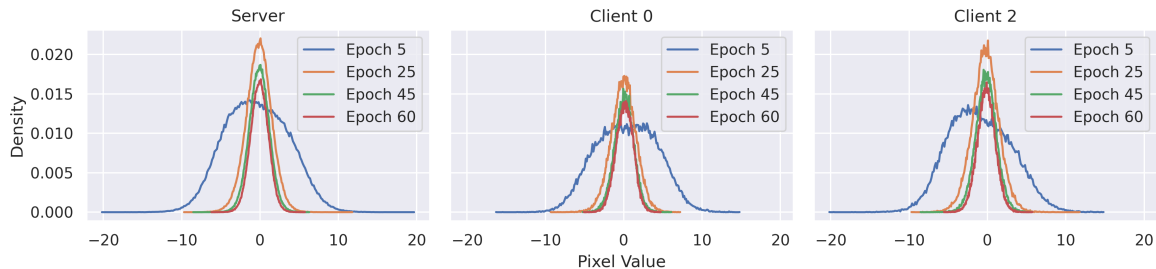


Figure 9. Pixel distribution of synthetic images at different stages. The synthetic images contain large pixel values at the earlier stage, implying the principle direction, and concentrate around zero later to focus on details. Meanwhile, the clients capture different statistics.

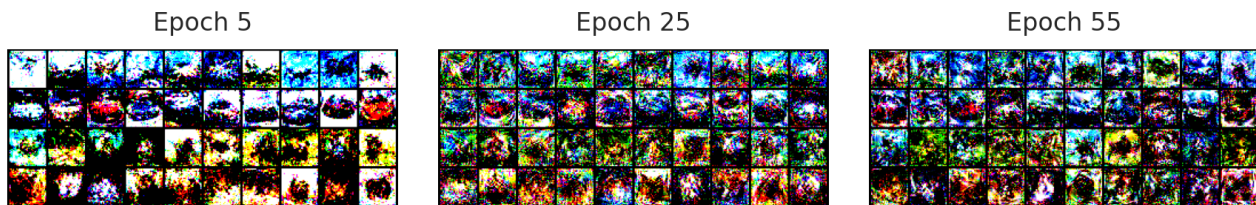


Figure 10. Visualization of synthetic images at the epochs 5, 25, and 55. We clip the pixel values to $[0, 1]$ and thus map extreme values to either white or black. It is observed that the images start from extreme values and gradually focus on details.

epochs 5, 25, 45, and 60. The synthetic images initially cover a wide range of values that could rapidly drive the model toward optimum and later concentrate on small values to carefully improve the utility. In addition, the distributions of clients behave drastically differently. Fig. 10 visualizes the corresponding images and matches the distributions. It is observed that at the beginning, the images contain the prototypes, such as cars, along with extreme values that are mapped to white or black. As training continues, they start focusing on details and introducing noise around zero to help with training. These observations provide more insights into training than traditional gradient-based methods and could open up possibilities toward accountability.

6. Discussion

Performance. Although we have shown that Fed-GLOSS facilitates federated optimization and saves communication costs, there is still a performance gap between our framework and pure FedAvg. Note that Fed-GLOSS’s main contribution is leveraging local approximation to perform global optimization. The framework can be further improved by advanced synthetic image generation algorithms, which is an ongoing research area (Zhao et al., 2021; Zhao and Bilen, 2023; Cazenavette et al., 2022). Additionally, not all dataset distillation algorithms work well with privacy-preserving federated learning since, as discussed in Sec 2, many rely on class-wise alignment. Making them compatible with FL and DP is still an open problem.

Accountability. Accountability is an emerging area of research in FL and might be required for trustworthy AI sys-

tems. However, it can conflict with privacy constraints that, e.g., prohibit direct access or auditing of the training data. Our framework, as shown in Sec. 5.6, presents that synthetic images and pixel distributions can capture the learning status changes, providing more insights into models that used to be challenging to investigate. These results may combine with interpretability methods in the image domain (Zhou et al., 2016; Selvaraju et al., 2017; Böhle et al., 2022) or distribution-based defences (Zheng and Hong, 2018) to audit training. We hope this work will inspire future work and open up possibilities toward reconciling privacy and accountability in FL.

7. Conclusion

This work proposes Fed-GLOSS-DP, a novel approach for privacy-preserving federated learning. Fed-GLOSS-DP uses synthetic samples to approximate the global loss landscape in a local neighborhood. This method optimizes according to the global objective and thereby mitigates issues with averaged, local gradients induced by non-IID private datasets, which prior gradient-sharing schemes struggle to address. Additionally, our method seamlessly integrates record-level DP, granting strong privacy protection for every data record. Extensive results show that Fed-GLOSS-DP surpasses the gradient-sharing counterparts in terms of faster and more stable convergence, up to 85% communication cost reduction, and reliable utility under DP settings. Lastly, we show that the synthesized images provide insights for training and present a new path toward reconciling privacy and accountability in federated learning.

Acknowledgment

This work was partially funded by the Helmholtz Association within the project "Trustworthy Federated Data Analytics (TFDA)" (ZT-I-OO1 4) and ELSA – European Lighthouse on Secure and Safe AI funded by the European Union under grant agreement No. 101070617. Views and opinions expressed are however those of the author(s) only and do not necessarily reflect those of the European Union or European Commission. Neither the European Union nor the European Commission can be held responsible for them. Dingfan Chen was partially supported by Qualcomm Innovation Fellowship.

References

- M. Abadi, A. Chu, I. Goodfellow, H. B. McMahan, I. Mironov, K. Talwar, and L. Zhang. Deep learning with differential privacy. In *Proceedings of the 2016 ACM SIGSAC conference on computer and communications security*, pages 308–318, 2016.
- B. Balle, G. Barthe, M. Gaboardi, J. Hsu, and T. Sato. Hypothesis testing interpretations and renyi differential privacy. In *International Conference on Artificial Intelligence and Statistics*, pages 2496–2506. PMLR, 2020.
- A. Bhowmick, J. Duchi, J. Freudiger, G. Kapoor, and R. Rogers. Protection against reconstruction and its applications in private federated learning. *arXiv preprint arXiv:1812.00984*, 2018.
- M. Böhle, M. Fritz, and B. Schiele. B-cos networks: Alignment is all we need for interpretability. In *Proceedings of the IEEE Conference on Computer Vision and Pattern Recognition (CVPR)*, pages 10329–10338, 2022.
- G. Cazenavette, T. Wang, A. Torralba, A. A. Efros, and J.-Y. Zhu. Dataset distillation by matching training trajectories. In *Proceedings of the IEEE Conference on Computer Vision and Pattern Recognition (CVPR)*, pages 4750–4759, 2022.
- D. Chen, R. Kerkouche, and M. Fritz. Private set generation with discriminative information. In *Advances in Neural Information Processing Systems (NeurIPS)*, 2022.
- C. Dwork, A. Roth, et al. The algorithmic foundations of differential privacy. *Foundations and Trends® in Theoretical Computer Science*, 9(3–4):211–407, 2014.
- J. Geiping, H. Bauermeister, H. Dröge, and M. Moeller. Inverting gradients-how easy is it to break privacy in federated learning? *Advances in Neural Information Processing Systems (NeurIPS)*, 33:16937–16947, 2020.
- Y. He, H.-P. Wang, and M. Fritz. Cossgd: Communication-efficient federated learning with a simple cosine-based quantization. In *1st NeurIPS Workshop on New Frontiers in Federated Learning (NFFL)*, 2021.
- B. Hitaj, G. Ateniese, and F. Perez-Cruz. Deep models under the gan: information leakage from collaborative deep learning. In *Proceedings of the 2017 ACM SIGSAC conference on computer and communications security*, pages 603–618, 2017.
- T.-M. H. Hsu, H. Qi, and M. Brown. Measuring the effects of non-identical data distribution for federated visual classification. *arXiv preprint arXiv:1909.06335*, 2019.
- P. Kairouz, H. B. McMahan, B. Avent, A. Bellet, M. Bennis, A. N. Bhagoji, K. Bonawitz, Z. Charles, G. Cormode, R. Cummings, et al. Advances and open problems in federated learning. *Foundations and Trends® in Machine Learning*, 14(1–2):1–210, 2021.
- S. P. Karimireddy, S. Kale, M. Mohri, S. Reddi, S. Stich, and A. T. Suresh. Scaffold: Stochastic controlled averaging for federated learning. In *International Conference on Machine Learning*. PMLR, 2020.
- R. Kerkouche, G. Acs, C. Castelluccia, and P. Genevès. Privacy-preserving and bandwidth-efficient federated learning: An application to in-hospital mortality prediction. In *Proceedings of the Conference on Health, Inference, and Learning*, pages 25–35, 2021.
- A. Khaled, K. Mishchenko, and P. Richtárik. First analysis of local gd on heterogeneous data. *arXiv preprint arXiv:1909.04715*, 2019.
- A. Krizhevsky, G. Hinton, et al. Learning multiple layers of features from tiny images. 2009.
- Y. LeCun, L. Bottou, Y. Bengio, and P. Haffner. Gradient-based learning applied to document recognition. *Proceedings of the IEEE*, 86(11):2278–2324, 1998.
- Y. LeCun, K. Kavukcuoglu, and C. Farabet. Convolutional networks and applications in vision. In *Proceedings of 2010 IEEE international symposium on circuits and systems*, pages 253–256. IEEE, 2010.
- Q. Li, B. He, and D. Song. Model-contrastive federated learning. In *Proceedings of the IEEE/CVF Conference on Computer Vision and Pattern Recognition*, pages 10713–10722, 2021.
- T. Li, A. K. Sahu, M. Zaheer, M. Sanjabi, A. Talwalkar, and V. Smith. Federated optimization in heterogeneous networks. *Proceedings of Machine Learning and Systems*, 2020a.
- X. Li, K. Huang, W. Yang, S. Wang, and Z. Zhang. On the convergence of fedavg on non-iid data. *arXiv preprint arXiv:1907.02189*, 2019.

- X. Li, M. JIANG, X. Zhang, M. Kamp, and Q. Dou. Fedbn: Federated learning on non-iid features via local batch normalization. In *International Conference on Learning Representations*, 2020b.
- M. Luo, F. Chen, D. Hu, Y. Zhang, J. Liang, and J. Feng. No fear of heterogeneity: Classifier calibration for federated learning with non-iid data. *Advances in Neural Information Processing Systems*, 34:5972–5984, 2021.
- B. McMahan, E. Moore, D. Ramage, S. Hampson, and B. A. y Arcas. Communication-efficient learning of deep networks from decentralized data. In *Proceedings of the International Conference on Artificial Intelligence and Statistics (AISTATS)*, pages 1273–1282. PMLR, 2017.
- L. Melis, C. Song, E. De Cristofaro, and V. Shmatikov. Exploiting unintended feature leakage in collaborative learning. In *2019 IEEE symposium on security and privacy (SP)*, pages 691–706. IEEE, 2019.
- I. Mironov. Rényi differential privacy. In *2017 IEEE 30th computer security foundations symposium (CSF)*, pages 263–275. IEEE, 2017.
- I. Mironov, K. Talwar, and L. Zhang. Rényi differential privacy of the sampled gaussian mechanism. *arXiv preprint arXiv:1908.10530*, 2019.
- M. Nasr, R. Shokri, and A. Houmansadr. Comprehensive privacy analysis of deep learning: Passive and active white-box inference attacks against centralized and federated learning. In *2019 IEEE symposium on security and privacy (SP)*, pages 739–753. IEEE, 2019.
- D. Peterson, P. Kanani, and V. J. Marathe. Private federated learning with domain adaptation. *arXiv preprint arXiv:1912.06733*, 2019.
- R. R. Selvaraju, M. Cogswell, A. Das, R. Vedantam, D. Parikh, and D. Batra. Grad-cam: Visual explanations from deep networks via gradient-based localization. In *Proceedings of the IEEE International Conference on Computer Vision (ICCV)*, pages 618–626, 2017.
- S. Truex, N. Baracaldo, A. Anwar, T. Steinke, H. Ludwig, R. Zhang, and Y. Zhou. A hybrid approach to privacy-preserving federated learning. In *Proceedings of the 12th ACM workshop on artificial intelligence and security*, 2019.
- H.-P. Wang, S. Stich, Y. He, and M. Fritz. ProgFed: effective, communication, and computation efficient federated learning by progressive training. In *Proceedings of the International Conference on Machine Learning (ICML)*, pages 23034–23054. PMLR, 2022.
- T. Wang, J.-Y. Zhu, A. Torralba, and A. A. Efros. Dataset distillation. *arXiv preprint arXiv:1811.10959*, 2018.
- H. Xiao, K. Rasul, and R. Vollgraf. Fashion-mnist: a novel image dataset for benchmarking machine learning algorithms. *arXiv preprint arXiv:1708.07747*, 2017.
- H. Yu, R. Jin, and S. Yang. On the linear speedup analysis of communication efficient momentum sgd for distributed non-convex optimization. In *International Conference on Machine Learning*. PMLR, 2019.
- B. Zhao and H. Bilen. Dataset condensation with distribution matching. In *Proceedings of the IEEE/CVF Winter Conference on Applications of Computer Vision*, pages 6514–6523, 2023.
- B. Zhao, K. R. Mopuri, and H. Bilen. Dataset condensation with gradient matching. *arXiv preprint arXiv:2006.05929*, 2020.
- B. Zhao, K. R. Mopuri, and H. Bilen. Dataset condensation with gradient matching. In *Proceedings of the International Conference on Learning Representations (ICLR)*, 2021.
- Z. Zheng and P. Hong. Robust detection of adversarial attacks by modeling the intrinsic properties of deep neural networks. *Advances in Neural Information Processing Systems (NeurIPS)*, 31, 2018.
- B. Zhou, A. Khosla, A. Lapedriza, A. Oliva, and A. Torralba. Learning deep features for discriminative localization. In *Proceedings of the IEEE Conference on Computer Vision and Pattern Recognition (CVPR)*, pages 2921–2929, 2016.

Appendix

A. Privacy Analysis

Definition A.1 (Rényi divergence). Let P and Q two distributions on \mathcal{X} defined over the same probability space, and let p and q be their respective densities. The Rényi divergence of a finite order $\alpha \neq 1$ between P and Q is defined as

$$D_\alpha(P \parallel Q) \triangleq \frac{1}{\alpha - 1} \ln \int_{\mathcal{X}} q(x) \left(\frac{p(x)}{q(x)} \right)^\alpha dx.$$

Rényi divergence at orders $\alpha = 1, \infty$ are defined by continuity.

Definition A.2 (Rényi differential privacy (RDP)). A randomized mechanism $\mathcal{M} : \mathcal{E} \rightarrow \mathcal{R}$ satisfies (α, ρ) -Rényi differential privacy (RDP) if for any two adjacent inputs $E, E' \in \mathcal{E}$ it holds that

$$D_\alpha(\mathcal{M}(E) \parallel \mathcal{M}(E')) \leq \rho$$

In this work, we call two datasets E, E' to be adjacent if $E' = E \cup \{x\}$ (or vice versa).

Definition A.3 (Sampled Gaussian Mechanism (SGM)). Let f be an arbitrary function mapping subsets of \mathcal{E} to \mathbb{R}^d . We define the Sampled Gaussian mechanism (SGM) parametrized with the sampling rate $0 < q \leq 1$ and the noise $\sigma > 0$ as

$$\text{SG}_{q,\sigma} \triangleq f(\{x : x \in E \text{ is sampled with probability } q\}) + \mathcal{N}(0, \sigma^2 \mathbb{I}^d),$$

where each element of E is sampled independently at random with probability q without replacement.

As for the Gaussian Mechanism, the sampled Gaussian mechanism consists of adding i.i.d Gaussian noise with variance σ^2 and zero mean to each coordinate value of the true output of f . In fact, the sampled Gaussian mechanism draws vector values from a multivariate spherical (or isotropic) Gaussian distribution which is described by random variable $\mathcal{N}(0, \sigma^2 \mathbb{I}^d)$, where d is omitted if it is unambiguous in the given context.

A.1. Analysis

The privacy guarantee of Fed-GLOSS-DP is quantified using the revisited moment accountant (Mironov et al., 2019) that restates the moments accountant introduced in Abadi et al. (2016) using the notion of Rényi differential privacy (RDP) defined in Mironov (2017).

Let μ_0 denote the pdf of $\mathcal{N}(0, \sigma^2)$ and let μ_1 denote the pdf of $\mathcal{N}(1, \sigma^2)$. Let μ be the mixture of two Gaussians $\mu = (1 - q)\mu_0 + q\mu_1$, where q is the sampling probability of a single record in a single round.

Theorem A.4. (Mironov et al., 2019). Let $\text{SG}_{q,\sigma}$ be the Sampled Gaussian mechanism for some function f and under the assumption $\Delta_2 f \leq 1$ for any adjacent $E, E' \in \mathcal{E}$. Then $\text{SG}_{q,\sigma}$ satisfies (α, ρ) -RDP if

$$\rho \leq \frac{1}{\alpha - 1} \log \max(A_\alpha, B_\alpha) \tag{18}$$

where $A_\alpha \triangleq \mathbb{E}_{z \sim \mu_0}[(\mu(z)/\mu_0(z))^\alpha]$ and $B_\alpha \triangleq \mathbb{E}_{z \sim \mu}[(\mu_0(z)/\mu(z))^\alpha]$

Theorem A.4 states that SGM applied to a function of l_2 -sensitivity 1 (but without loss of generality) satisfies α, ρ -RDP if $\rho \leq \frac{1}{\alpha - 1} \log \max(A_\alpha, B_\alpha)$. Thus, analyzing RDP properties of SGM is equivalent to upper bounding A_α and B_α .

From Corollary 7. in Mironov et al. (2019), $A_\alpha \geq B_\alpha$ for any $\alpha \geq 1$. Therefore, we can reformulate 18 as

$$\rho \leq \xi_{\mathcal{N}}(\alpha|q) = \frac{1}{\alpha - 1} \log A_\alpha \tag{19}$$

To compute A_α , we use the numerically stable computation approach proposed in Mironov et al. (2019) (Sec. 3.3) depending on whether α is expressed as an integer or a fractional.

Theorem A.5 (Composability (Mironov, 2017)). *Suppose that a mechanism \mathcal{M} consists of a sequence of adaptive mechanisms $\mathcal{M}_1, \dots, \mathcal{M}_k$ where $\mathcal{M}_i : \prod_{j=1}^{i-1} \mathcal{R}_j \times \mathcal{E} \rightarrow \mathcal{R}_i$. If all the mechanisms in the sequence are (α, ρ) -RDP, then the composition of the sequence is $(\alpha, k\rho)$ -RDP.*

In particular, Theorem A.5 holds when the mechanisms themselves are chosen based on the (public) output of the previous mechanisms. By Theorem 2, it suffices to compute $\xi_{\mathcal{N}}(\alpha|q)$ at each step and sum them to bound the RDP privacy budget of the mechanism overall.

Theorem A.6 (Conversion from RDP to DP (Balle et al., 2020)). *If a mechanism \mathcal{M} is (α, ρ) -RDP then it is $((\rho + \log((\alpha - 1)/\alpha) - (\log \delta + \log \alpha)/(\alpha - 1), \delta)$ -DP for any $0 < \delta < 1$.*

Theorem A.7 (Privacy of Fed-GLOSS-DP). *For any $0 < \delta < 1$ and $\alpha \geq 1$, Fed-GLOSS-DP is $(\min_\alpha (M \cdot \xi(\alpha|q_1) + M(T-1) \cdot \xi(\alpha|q_2) + \log((\alpha - 1)/\alpha) - (\log \delta + \log \alpha)/(\alpha - 1)), \delta)$ -DP, where $\xi_{\mathcal{N}}(\alpha|q)$ is defined in Eq. 19, $q_1 = \frac{C \cdot \mathbb{B}}{\min_k |\mathcal{D}_k|}$, and $q_2 = \frac{\mathbb{B}}{\min_k |\mathcal{D}_k|}$.*

The proof follows from Theorems A.4, A.5, A.6 and the fact that a record is sampled in the very first SGD iteration of every round if (1) the corresponding client is sampled, which has a probability of C , and (2) the batch sampled locally at this client contains the record, which has a probability of at most $\frac{\mathbb{B}}{\min_k |\mathcal{D}_k|}$. However, the adaptive composition of consecutive SGD iterations are considered where the output of a single iteration depends on the output of the previous iterations. Therefore, the sampling probability for the first batch is $q_1 = \frac{C \cdot \mathbb{B}}{\min_k |\mathcal{D}_k|}$, while the sampling probability for every subsequent SGD iteration within the same round is at most $q_2 = \frac{\mathbb{B}}{\min_k |\mathcal{D}_k|}$ conditioned on the result of the first iteration.

B. Algorithms

Distance metric Following existing works (Zhao et al., 2020; 2021), the distance \mathcal{L}_{dis} (in Equation 11 and 12 of the main paper) between the real and synthetic gradients is defined to be the sum of the cosine distance at each layer. Let $\mathbf{w}^{(l)}$ denote the weight at the l -th layer, the distance can be formularized as:

$$\mathcal{L}_{\text{dis}}(\nabla_{\mathbf{w}} \mathcal{L}(\mathbf{w}, \mathcal{D}_k), \nabla_{\mathbf{w}} \mathcal{L}(\mathbf{w}, \mathcal{S}_k)) = \sum_{l=1}^L d(\nabla_{\mathbf{w}^{(l)}} \mathcal{L}(\mathbf{w}^{(l)}, \mathcal{D}_k), \nabla_{\mathbf{w}^{(l)}} \mathcal{L}(\mathbf{w}^{(l)}, \mathcal{S}_k))$$

d denotes the cosine distance between the gradients at each layer:

$$d(\mathbf{A}, \mathbf{B}) = \sum_{i=1}^{\text{out}} \left(1 - \frac{\mathbf{A}_i \cdot \mathbf{B}_i}{\|\mathbf{A}_i\| \|\mathbf{B}_i\|} \right)$$

where \mathbf{A}_i and \mathbf{B}_i represent the flattened gradient vectors corresponding to each output node i . In FC layers, $\boldsymbol{\theta}^l$ is a 2D tensor with dimension $\text{out} \times \text{in}$ and the flattened gradient vector has dimension in , while in Conv layers, $\boldsymbol{\theta}^l$ is a 4D tensor with dimensionality $\text{out} \times \text{in} \times h \times w$ and the flattened vector has dimension $\text{in} \times h \times w$. Here we use out , in , h , w to denote the number of output and input channels, kernel height, and width, respectively.

Fed-GLOSS-DP We present the pseudocode of the Fed-GLOSS with record-level DP in Algorithm 2, which is supplementary to Sec. 4.4 of the main paper.

Algorithm 2 Fed-GLOSS-DP

function ServerExecute:

Initialize global weight $\mathbf{w}_g^{1,1}$, Fix the radius r
/ Local approximation */*
for $m = 1, \dots, M$ **do**
for $k = 1, \dots, K$ **do**
 $\mathcal{S}_k \leftarrow \text{ClientsExecute}(k, r, \mathbf{w}_g^{m,1})$
end for
/ Global optimization */*
 $t \leftarrow 1$
while $\|\mathbf{w}_g^{m,1} - \mathbf{w}_g^{m,t}\| < r$ **do**
 $\mathbf{w}_g^{m,t+1} = \mathbf{w}_g^{m,t} - \sum_{k=1}^K \eta \frac{N_k}{N} \nabla_{\mathbf{w}} \mathcal{L}(\mathbf{w}_g^{m,t}, \mathcal{S}_k)$
 $t \leftarrow t + 1$
end while
 $\mathbf{w}_g^{m+1,1} \leftarrow \mathbf{w}_g^{m,t}$
end for
Return: global model weight $\mathbf{w}_g^{M+1,1}$
function ClientExecute($k, r, \mathbf{w}_g^{m,1}$):

Initialize \mathcal{S}_k : $\{\hat{\mathbf{x}}_k^m\}$ from Gaussian noise or $\{\hat{\mathbf{x}}_k^{m-1}\}$, $\{\hat{y}_k\}$ to be a balanced set

for $i = 1, \dots, R_i$ **do**
/ Resample training trajectories */*

 Reset $t \leftarrow 1$ and model $\mathbf{w}_k^{m,1} \leftarrow \mathbf{w}_g^{m,1}$
while $\|\mathbf{w}_k^{m,t} - \mathbf{w}_k^{m,1}\| < r$ **do**

 Uniformly sample random batch $\{(\mathbf{x}_k^i, y_k^i)\}_{i=1}^{\mathbb{B}}$ from \mathcal{D}_k
for each (\mathbf{x}_k^i, y_k^i) **do**
/ Compute per-example gradients on client data */*
 $g^{\mathcal{D}}(\mathbf{x}_k^i) = \nabla_{\mathbf{w}} \ell(\mathbf{w}_k^{m,t}, \mathbf{x}_k^i, y_k^i)$
/ Clip gradients with bound \mathbb{C} */*
 $\widetilde{g}^{\mathcal{D}}(\mathbf{x}_k^i) = g^{\mathcal{D}}(\mathbf{x}_k^i) \cdot \min(1, \mathbb{C} / \|g^{\mathcal{D}}(\mathbf{x}_k^i)\|_2)$
end for
/ Add noise to average gradient by Gaussian mechanism */*

 Compute $\nabla \widetilde{\mathcal{L}}(\mathbf{w}_k^{m,t}, \mathcal{D}_k) = \frac{1}{\mathbb{B}} \sum_{i=1}^{\mathbb{B}} (\widetilde{g}^{\mathcal{D}}(\mathbf{x}_k^i) + \mathcal{N}(0, \sigma^2 \mathbb{C}^2 I))$
for $j = 1, \dots, R_b$ **do**
/ Update synthetic set \mathcal{S}_k */*
 $\mathcal{S}_k = \mathcal{S}_k - \tau \nabla_{\mathcal{S}_k} \mathcal{L}_{dis}(\nabla \widetilde{\mathcal{L}}(\mathbf{w}_k^{m,t}, \mathcal{D}_k), \nabla \mathcal{L}(\mathbf{w}_k^{m,t}, \mathcal{S}_k))$
end for
for $l = 1, \dots, R_l$ **do**
/ Update local model parameter \mathbf{w}_k */*
 $\mathbf{w}_k^{m,t+1} = \mathbf{w}_k^{m,t} - \eta \nabla \mathcal{L}(\mathbf{w}_k^{m,t}, \mathcal{S}_k)$
 $t \leftarrow t + 1$
end for
end while
end for
Return: Synthetic set \mathcal{S}_k